

MRI noise estimation and denoising using non-local PCA

José V. Manjón^a, Pierrick Coupé^b, Antonio Buades^c

jmanjon@fis.upv.es, pierrick.coupe@labri.fr, toni.buades@uib.es

^a Instituto de Aplicaciones de las Tecnologías de la Información y de las Comunicaciones Avanzadas (ITACA), Universidad Politécnica de Valencia, Camino de Vera s/n, 46022 Valencia, Spain

^b Laboratoire Bordelais de Recherche en Informatique, Unité Mixte de Recherche CNRS (UMR 5800), PICTURA Research Group, 351, cours de la Libération F-33405 Talence cedex, France.

^c Dpt Matemàtiques i Informàtica, Universitat Illes Balears, Ctra Valldemossa km 7.5, 07122 Palma de Mallorca, Spain.

* Corresponding author: José V. Manjón. Instituto de Aplicaciones de las Tecnologías de la Información y de las Comunicaciones Avanzadas (ITACA), Universidad Politécnica de Valencia, Camino de Vera s/n, 46022 Valencia, Spain

Tel.: (+34) 96 387 70 00 Ext. 75275, Fax: (+34) 96 387 90 09

E-mail: jmanjon@fis.upv.es (José V. Manjón)

Keywords: MRI, PCA, denoising, sparseness, non-local means

Abbreviations:

PCA: Principal Component Analysis

NLM: Non Local Means

PSNR: Peak signal to Noise Ratio

RMSE: Root mean squared error

SSIM: Structural similarity index

Abstract

This paper proposes a novel method for MRI denoising that exploits both the sparseness and self-similarity properties of the MR images. The proposed method is a two-stage approach that first filters the noisy image using a non local PCA thresholding strategy by automatically estimating the local noise level present in the image and second uses this filtered image as a guide image within a rotationally invariant non-local means filter. The proposed method internally estimates the amount of local noise presents in the images that enables applying it automatically to images with spatially varying noise levels and also corrects the Rician noise induced bias locally. The proposed approach has been compared with related state-of-the-art methods showing competitive results in all the studied cases.

1. Introduction

Magnetic resonance (MR) imaging has very important role on current medical and research procedures. However, these images are inherently noisy and thus filtering methods are required to improve the data quality. This denoising process is usually performed as a preprocessing step in many image processing and analysis tasks such as registration or segmentation.

There is a large amount of bibliography related to the denoising topic that highlights the relevance of this issue for the scientific community. A large review of MRI denoising methods can be found at [Mohan et al \(2014\)](#). Currently, most denoising methods can be classified on those that use the intrinsic pattern redundancy of the data and those exploiting their sparseness properties.

On the first class, the well known non-local means (NLM) filter ([Buades et al,2005](#)) is maybe the most representative method. This method reduces the noise by exploiting the self-similarity of the image patterns by averaging similar image patterns. In MRI, early works using the NLM method are from [Coupe et al \(2008\)](#) and [Manjón et al \(2008\)](#). The bibliography related to this method is quite extensive ([Tristan-Vega et al, 20012](#); [Coupe et al., 2012](#); [Manjón et al., 2009, 2010, 2012](#); [Wiest-Daesslé et al, 2008](#); [He and Greenshields, 2009](#); [Rajan et al. 2012, 2014](#)).

On the other hand, sparseness-based methods try to reduce the noise naturally present in the images by assuming that the noisy data can be represented in a lower dimensionality space. In such methods, it is considered that most of the signal can be sparsely represented using few bases that enables to discard the noise related components or simply approximate noisy patterns by their corresponding noise free patterns. An example of these techniques are for instance those based on FFT or DCT transforms where standard bases such as sin or cosine functions are used to represent the images ([Guleryuz, 2003](#); [Yaroslavsky et al., 2000](#)). In this case, noise reduction is achieved by removing noise related coefficients in a transform domain using either soft or hard thresholding techniques. More recently, techniques that learn the bases from the images to be denoised have received much attention ([Elad et al. 2006](#), [Mairal et al.,2008](#); [Protter et al.,2009](#)). These techniques learn a set of bases from the images to be denoised or from a set of similar noise free images to create a dictionary to sparsely represent image patches as a linear combination of dictionary entries ([Aharon et al. 2006](#)). The advantage of these dictionaries over standard ones such those used on DCT or FFT transforms is the fact they are better adapted to the images to be processed that enables a sparser representation and therefore a better signal/noise separation. In MRI, sparse theory has been used in many recent methods ([Bao et al.2008](#); [Bao et al. 2013](#); [Pattel et al.2011](#)).

Principal Component Analysis (PCA) and related approaches have been also used for noise reduction in images ([Muresan et al., 2003](#); [Bydder et al., 2003](#); [Deledalle et al., 2011](#)). This type of technique falls in the second category since it takes benefit from the fact that original signal can be projected into an orthogonal space where most of the variance of the signal is

accumulated in few components while the noise being not sparse is uniformly spread over all the components. Noise reduction using PCA normally requires 3 main steps: 1) decomposing a set of selected signals into their principal components, 2) shrinking noise related components, and finally 3) reconstructing back the signals by inverting the PCA decomposition. This approach was first used by [Muresan et al \(2003\)](#) by applying PCA decomposition over a local set of image patches. [Zhang et al. \(2010\)](#) improved this approach by grouping similar patches before PCA decomposition and iterated the process to obtain a higher noise reduction. PCA has been also used to robustly compute patch similarities within a Non-local means framework ([Van de Ville and Kocher, 2010](#); [Zhang et al., 2013](#); [Zhang et al., 2014](#)).

PCA based denoising has been also used for MRI filtering. In [Manjón et al. \(2009\)](#) PCA was used as a postprocessing step to remove remaining noise after the application of a multicomponent non-local means filter for multimodal MRI. Recently, a nonparametric PCA based filter was proposed for 2D MR images where patch similarities are estimated using rank limited PCA coefficients ([Kim et al., 2010](#)). Also recently, PCA based approaches have been proposed for diffusion weighted image (DWI) denoising ([Bao et al., 2013](#); [Fan et al., 2013](#); [Manjón et al., 2013](#)).

In this paper, we present a novel denoising approach based on the application of PCA decomposition over a set of similar patches using a sliding window scheme. The resulting filtered image is used as a guide image to accurately estimate the voxel similarities within a rotationally invariant NLM (PRI-NLM) strategy as done in [Manjón et al. \(2012\)](#). The increased quality of this guide image resulting from the proposed PCA-based noise removal method significantly improves the application of the PRI-NLM filter boosting the overall denoising performance. We must remark that our guided PRI-NLM filter shares some similarities with methods like the one proposed by [Salmon et al. \(2012\)](#) where a Yaroslasky filter is applied using information from a pre-filtered image to improve denoising performance or also CANDLE filter ([Coupe et al., 2012](#)) which uses a median filtered image. Our approach is also related the method proposed by [Zhang et al. \(2010\)](#) to filter natural images with stationary Gaussian noise but in our case our patch selection is performed on a pre-filtered image to obtain a more robust patch grouping on very noisy conditions. Furthermore, we deal with non-stationary Rician noise and the thresholding step is performed by automatically estimating the local noise level from the eigenvalues of the PCA decomposition. The three main contributions in this paper are: 1) a new collaborative filter using a PCA based strategy to compute an improved guide image. 2) an automatic spatially varying noise estimation method fully integrated in the denoising pipeline and 3) a new Rician bias correction method.

2. Material and methods

Principal component analysis is a mathematical procedure that uses an orthogonal linear transformation to map the data into a new coordinate system where all the components are sorted by decreasing variance order. PCA has been traditionally used for dimensionality reduction but during the last decade some filtering applications have been proposed (Muresan et al., 2003; Bydder et al., 2003). The main idea when using PCA for noise reduction is to use its decorrelation properties to separate the signal from the noise by applying it to a set of noisy observations in order to erase least significant components that are mainly noise related.

2.1. Non-local PCA denoising

In this paper we present a novel method related with the filter proposed by Zhang et al (2010) where similar patches are grouped together prior performing the PCA decomposition. Differently from Zhang et al. (2010) (which was developed for natural images with stationary Gaussian noise) we group similar patches using a pre-filtered guide image that improves the group selection process in noisy conditions yielding in a sparser group definition. Besides, we have made our proposed method fully adaptive by internally estimating the local amount of noise within each group of patches.

By using the usual definition of denoising problem, let define a noisy image Y as the original noise free signal A plus some noise N :

$$Y = A + N \quad (1)$$

The aim of any denoising method is to estimate A given Y .

In our proposed approach we use a sliding 3D window approach where for each 3D patch of the image volume we create a group of patches by selecting the most similar patches to the current patch in a local search volume surrounding it. Specifically, for each point x_i of the image domain $\Omega \subset \mathbb{R}^3$, a set of the N most similar 3D patches (in the Euclidean distance sense) within a search volume (cube of $(2t+1)^3$ voxels) surrounding x_i are reordered as a row vector in a matrix X (see figure 1). X is thus an $N \times K$ matrix where K corresponds to the number of voxels of each 3D patch and N the number of grouped patches (in our method we set $N=k$).

For every created group of similar patches, PCA decomposition is then performed and the less significant components are erased using a hard thresholding rule (i.e., eigenvectors with a standard deviation lower than a threshold τ are set to zero). Finally, since each voxel has contributions from different patches all estimates are combined using a uniform averaging rule. We will refer this method as Non-local PCA (NL-PCA) filter.

The homogeneity of the group plays a very important role in the denoising process since more homogeneous groups will provide sparser representations and therefore will enable a better noise reduction. To this end, instead of comparing noisy patches for the group selection we

propose to use a pre-filtered volume to drive the selection process. We found that a simple 3D median filter significantly improves the patch selection during grouping process (especially for medium and high noise levels). Therefore, as done in (Coupe et al., 2012), we used a simple 3D median filter due to its efficiency and because it can be applied automatically without any knowledge of the local noise level present at each point of the images.

Finally, another important feature of our proposed method is its ability to automatically estimate the noise statistics from each group of patches. In this sense, the algorithm naturally adapts to spatially varying noise patterns and it is actually independent of any external noise estimation method (this issue will be discussed in the section 2.4).

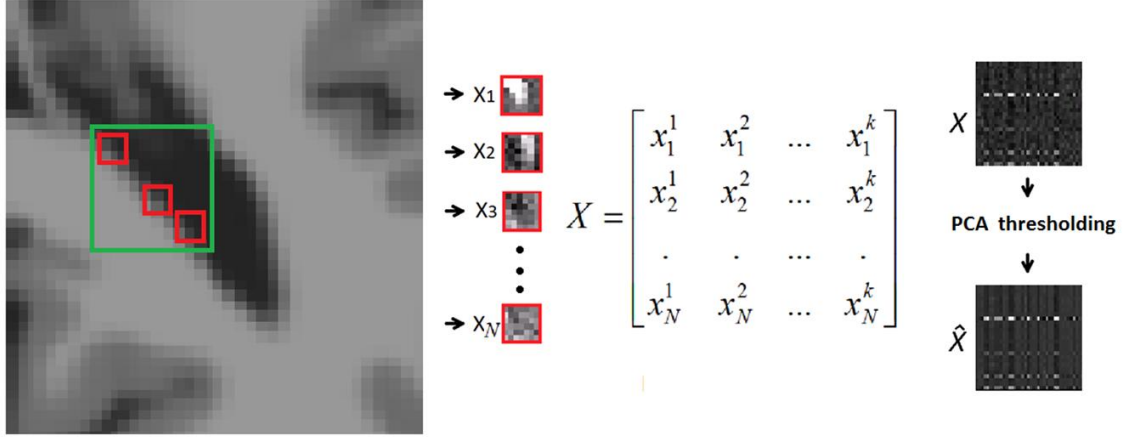


Figure 1. Overview of NL-PCA scheme. A set of N similar patches are selected to create a matrix X . This matrix is then transformed using PCA and the least significant eigenvectors are removed by hard thresholding. Finally, the filtered matrix X is obtained by inverting the PCA decomposition.

2.2. Rotational Invariant Non- local PCA denoising

As demonstrated in Manjón et al. (2012), when a good quality pre-filtered image is available we can use this image to guide the similarity estimation process of a rotationally invariant version of the NLM filter.

$$\hat{A}(i) = \frac{\sum_{j \in \Omega} w(i, j) y(j)}{\sum_{j \in \Omega} w(i, j)} \quad w(i, j) = e^{-\frac{1}{2} \left(\frac{(g(i) - g(j))^2 + 3(\mu_{N_i} - \mu_{N_j})^2}{2h_i^2} \right)} \quad (2)$$

where μ_{N_i} and μ_{N_j} are the mean values of patches N_i and N_j around voxels i and j in the guide image g , h is related to the standard deviation of the noise present on image y and Ω represents position of the elements of the search volume. We refer the reader to the original paper (Manjón et al. 2012) to see the details of the rotational invariant NLM filter.

In this previous work, the pre-filtered image was estimated using a local DCT based filter while in this paper we propose to use the output of the described NL-PCA filter as guide image. We

will refer to this filter as PRI-NL-PCA to differentiate it from the PRI-NLM proposed in our previous work (Manjón et al. 2012).

It is worth noting that applying this rotational invariant NLM using the NL-PCA guide image outperforms the re-application of NL-PCA using the NL-PCA output of the first iteration as guide image.

2.3. Adaptation to Rician noise

Contrary to the usual denoising problem in natural images where noise is considered as Gaussian, noise in magnitude MR images normally follows a Rician distribution (Nowak et al., 1999). The asymmetry of the Rician distribution results in a non-constant intensity bias as it depends on the local SNR. To reduce such bias, some authors have proposed to remove the bias in the squared magnitude image (Wiest-Daesslé et al., 2008, Manjón et al., 2008).

However, this approach can be applied only when reducing the noise using the averaging principle. In our case, due to the effect of PCA thresholding, the bias in the squared domain is not constant, but intensity dependent. Fortunately, this bias can be estimated theoretically and inverted in the original domain using the properties of the first moment of a Rician distribution as done in Manjón et al. (2013).

This correction algorithm is used to recover the mean value of the Rice distribution $R(v, \sigma)$ with parameters v and σ , being v the true value we want to recover and σ the noise standard deviation. The expected value writes as:

$$E[R(v, \sigma)] = \sigma \sqrt{\frac{\pi}{2}} \exp\left(-\frac{v^2}{2\sigma^2}\right) \left(\left(1 + \frac{v^2}{2\sigma^2}\right) I_0\left(\frac{v^2}{4\sigma^2}\right) + \left(\frac{v^2}{2\sigma^2}\right) I_1\left(\frac{v^2}{4\sigma^2}\right) \right)^2 \quad (3)$$

where I_0 and I_1 are the modified Bessel functions of order zero and one, respectively.

After denoising the data using the proposed NL-PCA method and knowing the noise variance, we can compensate for the bias by inverting the previous expression and recovering the true value v . We can observe that $E[R(v, \sigma)]/\sigma$ can be written as a function of $\phi = v/\sigma$.

$$\frac{E[R(v, \sigma)]}{\sigma} = \sqrt{\frac{\pi}{2}} \exp\left(-\frac{\phi^2}{2}\right) \left(\left(1 + \frac{\phi^2}{2}\right) I_0\left(\frac{\phi^2}{4}\right) + \left(\frac{\phi^2}{2}\right) I_1\left(\frac{\phi^2}{4}\right) \right)^2 \quad (4)$$

The inverse of this expression as a function of ϕ can be stored into a Look Up Table (LUT) that we denote by $\eta(\phi)$. The final estimated value x obtained by the denoising process with this bias correction can be written as:

$$\hat{x} = \sigma \eta(x/\sigma) \quad (5)$$

The Rician bias correction for the RI-NL-PCA method is performed in squared magnitude image as done in the RI-NLM method (Manjón et al., 2013).

$$\hat{A}(i) = \sqrt{\max\left(\left(\frac{\sum_{j \in \Omega} w(i, j) y(i)^2}{\sum_{j \in \Omega} w(i, j)}\right) - 2\sigma(i)^2, 0\right)} \quad (6)$$

Where in this case the fixed bias $2\sigma(i)^2$ depends on the local noise level $\sigma(i)$ at position i .

We should note that the presented bias correction techniques can be applied to single coil or SENSE acquired images but not to GRAPPA acquired images. In this case, the noise distribution does not follow a Rician distribution but a Non-central Chi distribution. However, we can modify equation 6 to take into account noise contribution of each of the multiple N coils.

$$\hat{A}(i) = \sqrt{\max\left(\left(\frac{\sum_{j \in \Omega} w(i, j) y(i)^2}{\sum_{j \in \Omega} w(i, j)}\right) - 2N\sigma(i)^2, 0\right)} \quad (7)$$

Here, N represents the number of coils used in the GRAPPA acquisition. In this paper, we will perform the experiments on Rician noise to focus on denoising methodology rather on the nature of noise in MRI.

2.4. PCA based noise estimation

The NL-PCA method relies heavily on the correct estimation of the optimum threshold to select the signal related components. This threshold is normally set as function of the noise level present on the image. Therefore, a good noise level estimation is fundamental to obtain an optimal filtering performance.

Although, there are several methods to estimate the noise level in MRI (Sijbers et al., 2007; Coupe et al., 2010; Aja et al., 2009; Pyatykh et al., 2013) most of them assume a stationary condition of the noise (i.e., the noise level is the same over the entire image) that is not a valid assumption when using images acquired with parallel imaging techniques such as SENSE. As far as we know only two methods has been presented for non-stationary noise estimation in MRI. The first is the approach of Pan et al. (2012) based on local kurtosis measures and designed for Gaussian distributed noise, and the second is the Maggioni and Foi method (2013) which is based on local DCTs and is able to deal with Rician noise.

In this paper we propose a new method for local noise estimation which is fully integrated within the proposed NL-PCA method.

The eigenvalues of the PCA decomposition represents the variability of both signal and noise contributions at each component. First components are mainly related to signal while last components are mainly related to noise. This fact has been used to reduce noise by using hard thresholding techniques like the one presented in this paper.

When a set of similar patches are grouped together prior to perform PCA decomposition, the resulting set is expected to be highly sparse due to the high level of pattern redundancy within the group of selected patches. Therefore, we can assume that most of the signal contribution will be concentrated in the first components while the remaining components will be mainly dominated by the noise. If the set of selected patches belong to a homogeneous area the mean of the eigenvalues is expected to be close to the variance of the noise (the same holds for the median of the eigenvalues). However, if our set of patches corresponds to edges or textured areas, the mean of the eigenvalues will logically overestimate the noise variance due to signal variance contamination. However, if our representation is sparse enough, the median of the eigenvalues still will provide a robust noise level estimator (see Figure 2).

Although the median of the eigenvalues is related to the noise variance, there is a systematic bias that depends on the relation between the number of selected patches and the number of voxels of each patch. Therefore, the local noise standard deviation can be derived from the median of the eigenvalues using the following expression:

$$\hat{\sigma} = \beta \sqrt{\text{median}(\lambda)} \quad (8)$$

where β corresponds to the correction factor related to the ratio between the number of selected patches and the number of voxels of each patch ($\beta = 1.16$ for $N=K$ which was experimentally obtained by numerical simulation) and λ represents the eigenvalues of the PCA decomposition. A theoretical correction factor being close to β can be estimated when all the selected patches are equal up to the noise. In that case, the PCA eigenvalues follow a known distribution depending on the ratio N/K and the noise standard deviation σ , which permits to analytically compute this correction factor. This theoretical factor slightly differs from the one used, since in practice the N patches are not always identical up to noise oscillations.

Although this simple method provides accurate estimates for medium and high noise levels it tends to slightly overestimate the noise level for low noise conditions at areas with low pattern redundancy and strong edges (i.e. low group sparseness). The reason for this overestimation is the fact that for low noise levels the variance of the signal may be non negligible compared to the variance of the noise at the eigenvalue median. To minimize the impact of the signal in the noise estimation we can estimate the noise level only from a subset of the eigenvalues by

adaptively removing some of the first eigenvalues prior the median estimation. To do so, we remove the eigenvalues with a standard deviation higher than two times the standard deviation of the median of the full set of eigenvalues. We finally estimate the noise standard deviation as the square root of the median of this trimmed subset of eigenvalues but using the corresponding correction factor ($\beta = 1.29$) taking into account the reduced size of the subset of selected eigenvalues.

$$\hat{\sigma} = \beta \sqrt{\text{median}(\lambda_t)} \quad \lambda_t = \{\lambda_i \mid \sqrt{\lambda_i} < 2 \text{median}(\sqrt{\lambda})\} \quad (9)$$

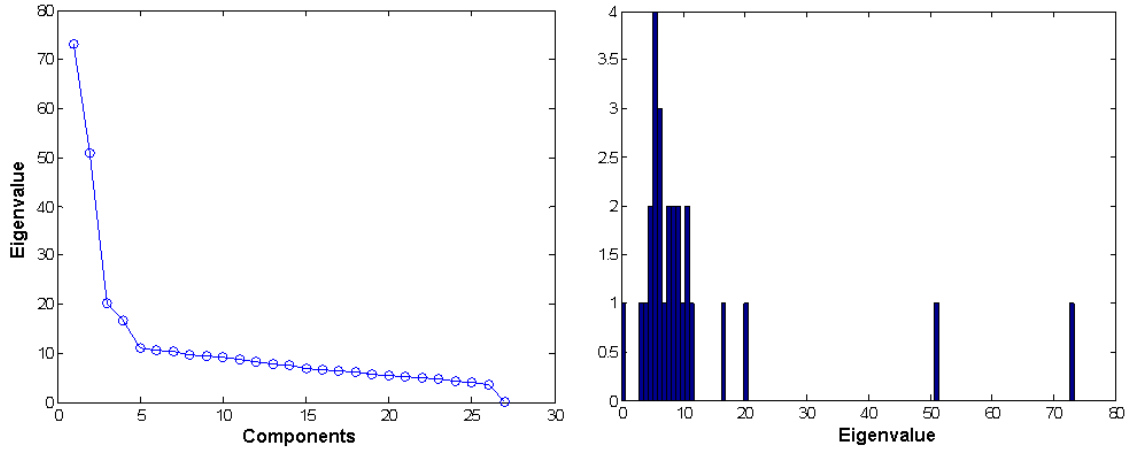


Figure 2. Left: Example of PCA eigenvalues (observe that most of the signal variance comes from the first 4 eigenvalues). Right: Histogram of the eigenvalue distribution (notice that first eigenvalues can be identified as outliers of the noise related components distribution). The noise variance in this example case was around 7.

Rician noise estimation

The above described noise estimation methods rely on a Gaussian nature assumption of the noise. However, as previously commented, it is well known that magnitude MRI noise normally follows a Rician distribution. Therefore, the presented noise estimation approach has to be adapted to deal with this fact. One approach that has been successfully used in the past for correcting the noise underestimation at low SNR areas is based on the iterative analytical correction scheme proposed by [Koay and Basser \(2006\)](#). This approach was used for stationary noise estimation in MRI ([Coupe et al., 2010](#); [Manjón et al., 2010](#)).

However, we have experimentally observed that this approach although effective to estimate the global noise level does not provides optimal results when used locally, probably due to convergence problems in the iterative process for very low SNR areas.

As an alternative, we propose in this paper a simple but efficient and accurate method to map Gaussian-like local estimates in their corresponding Rician ones by using the effective local SNR instead of the estimated SNR as used by [Koay and Baser \(2006\)](#).

We estimated a mapping function correcting the systematic noise underestimation by using Monte-Carlo simulations where effective local SNR (that is the ratio between the local mean and the corresponding local standard deviation) was related to the correction factor that converts the local Gaussian-like standard deviation to the corresponding Rician one (see Figure 3). We fitted the simulated data using the following rational model.

$$\Phi(\gamma) = \begin{cases} \frac{((0.9846(\gamma - 1.86) + 0.1983))}{((\gamma - 1.86) + 0.1175))} & \text{if } (\gamma > 1.86) \\ 0 & \text{otherwise} \end{cases} \quad (10)$$

where γ represents the effective local SNR. The corrected local standard deviation is calculated by multiplying the correction factor based on the effective local SNR with the initially estimated local standard deviation provided by the NL-PCA method.

$$\hat{\sigma} = \sigma \Phi(\gamma) \quad (11)$$

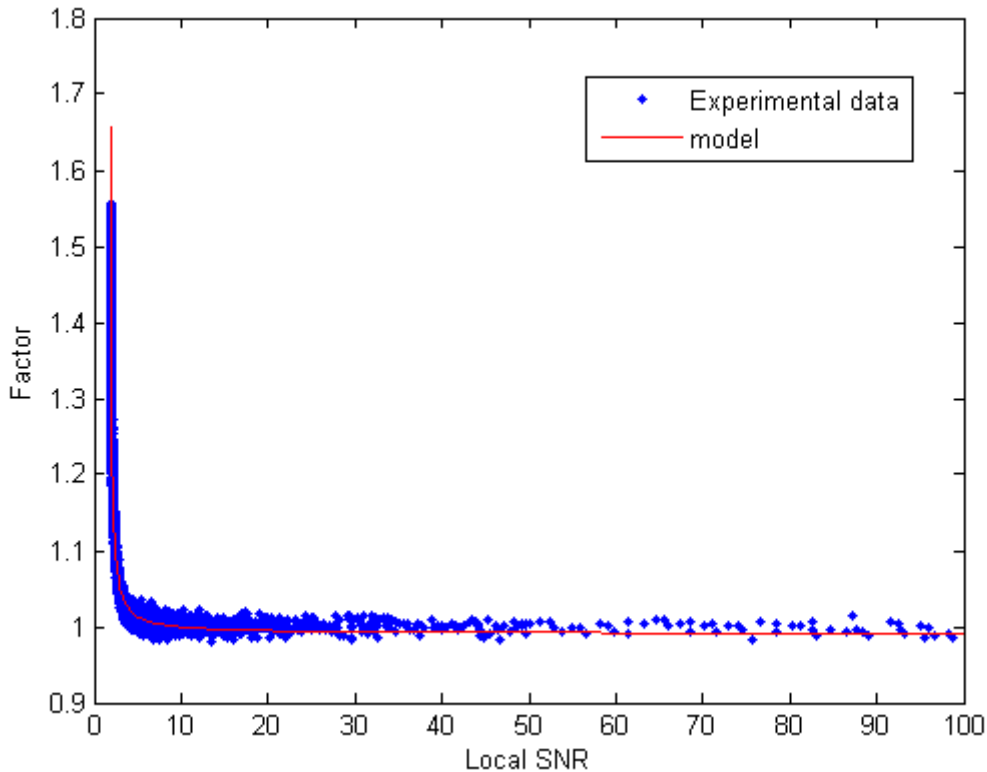


Figure 3. Experimental noise correction factors for different SNR values and its associated model. As can be noted, the correction factor for high SNR is close to 1 as expected while for low SNR its value increases to counteract the noise underestimation.

Finally, to further improve the Rician noise estimation required to apply bias correction to the NL-PCA filter and to provide accurate noise estimation to the PRI-NL-PCA method, we apply a low-pass filter to the estimated noise map. We do so to further regularize the estimated spatially varying noise field to produce a more realistic noise map (the noise field is expected to be slowly varying). We have used a kernel size of 15 mm^3 for that purpose. In the case that the noise is found to be constant across the entire image, the average of all local estimations can be used to provide a more accurate estimation. To detect this homogeneity condition we used coefficient of variation (CoV) of the estimated noise field (the stationary condition was met for $\text{CoV} < 0.15$). In table 1 we summarize the described NL-PCA and PRI-NL-PCA methods.

Table 1. Summary of the proposed methods.

Method NL-PCA	Method PRI-NL-PCA
<ol style="list-style-type: none"> 1. Estimate guide image (3D median filter) 2. For each 3D patch: <ol style="list-style-type: none"> 2.1. Group similar non-local patches 2.2. Perform PCA decomposition 2.3. Estimate local noise level (Eq. 9) 2.4. Perform hard thresholding 2.5. Invert PCA decomposition 3. Combine multiple voxel contributions to obtain the denoised images and the estimated noise field. 4. Correct Rician bias on the filtered images using Eq. 5 and correct Rician noise field estimation using Eq. 11. 	<p>Stage 1 (Basic estimate)</p> <ul style="list-style-type: none"> • Perform NL-PCA filtering <p>Stage 2 (Final estimate)</p> <ul style="list-style-type: none"> • Apply PRI-NLM filter over the noisy image using as guide image the filtered image and the estimated noise field obtained from NL-PCA filter.

3. Experiments and results

Several experiments were carried out to estimate the optimal filter settings as well as to compare the proposed methods to related *state-of-the-art* methods.

3.1. Experimental data description

For our experiments, we used the well-known Brainweb 3D T1-weighted (T1w) MRI phantom (Collins et al., 1998; Kwan et al., 1999). This dataset has a size of 181×217×181 voxels (voxel resolution = 1 mm³) and it was corrupted with different levels of Gaussian and Rician noise (1% to 9% of maximum intensity). Rician noise was generated by adding Gaussian noise to real and imaginary parts and then computing the magnitude image.

Two quality measures were used to evaluate the results. The first was the Peak Signal to Noise Ratio (PSNR) metric while the second was the structural similarity index (SSIM) (Wang et al., 2004), which is a measure more consistent with the human visual system:

$$SSIM(x, y) = \frac{(2\mu_x\mu_y)(2\sigma_{xy} + c_2)}{(\mu_x^2 + \mu_y^2 + c_1)(\sigma_x^2 + \sigma_y^2 + c_2)}, \quad (12)$$

where μ_x and μ_y are the mean value of images x and y , σ_x and σ_y are the standard deviation of images x and y , σ_{xy} is the covariance of x and y , $c_1 = (k_1L)^2$, and $c_2 = (k_2L)^2$ (where L is the dynamic range, $k_1 = 0.01$ and $k_2 = 0.03$). As suggested by Wang et al. (2004), the SSIM was locally estimated using a Gaussian kernel of 3×3×3 voxels. Finally, the mean value of all the local estimations was used as a quality metric. For the sake of clarity, both measures were estimated only in the region of interest (head tissues) discarding the background.

3.2. Parameter estimation

The proposed NL-PCA method has several free parameters that need to be set to obtain optimal performance.

The three most important parameters of the proposed method are the 3D Patch side size r (so $k=r^3$), the search volume radius t and the threshold τ applied to local PCA eigenvalues to erase the noise related components. To find the optimum values of these parameters an exhaustive search was performed. In figure 4 (left) the mean PSNR (for all noise levels) in function of the threshold τ is plotted for 3 different patch sizes. As can be noted, optimum results are found for $r=4$ and $\tau=2.1\sigma$ for the PRI-NL-PCA and $\tau=2.2\sigma$ for NL-PCA. Also in figure1 (right) the mean PSNR in function of the search volume radius t is plotted (in this case we fixed $r=4$ and $\tau=2.1\sigma$).

As can be observed optimum results are obtained for a search volume radius value of $t=3$ (i.e., a search volume of size $7 \times 7 \times 7$ voxels). Gaussian noise was used in these experiments to simplify the analysis of the results. From these experiments, we set as default parameters $r=4$ (Patch of $4 \times 4 \times 4$ voxels), $\tau=2.1\sigma$ and $t=3$ (search volume size of $7 \times 7 \times 7$ voxels). These parameters are used in all the following experiments.

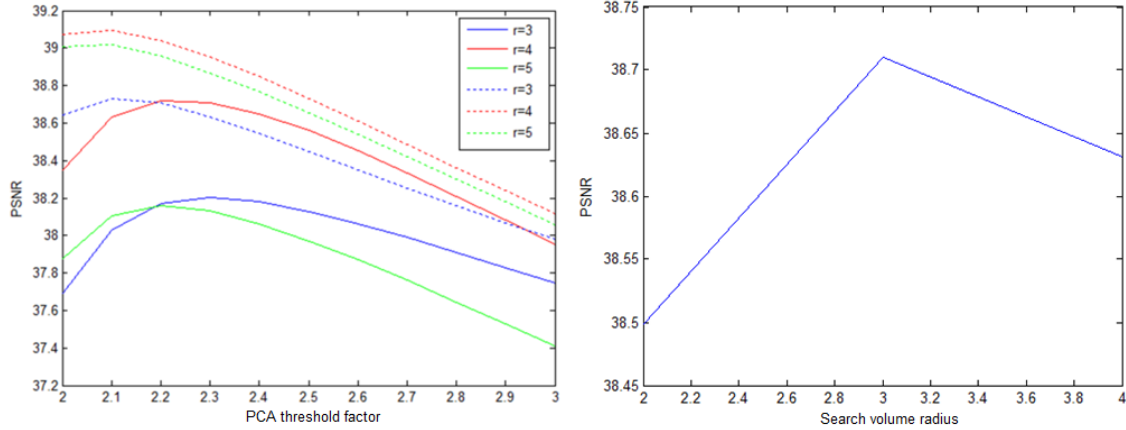


Figure 4. Left: PSNR results for different values of threshold τ and patch sizes. Solid lines correspond to NL-PCA results while dashed lines correspond to PRI-NL-PCA results. Right: Mean PSNR results for NL-PCA method for 3 different values of search volume radius. Optimum results were found at $t=3$.

These results were obtained using a sliding window approach with full overlap over consecutive patches (no gap between consecutive windows) as it is known that overcomplete approaches enable to obtain better denoising results by increasing the number of elements contributing to every voxel from the different overlapping denoised patches as demonstrated by [Katkovnik et al. \(2010\)](#). However, we analyzed the effect of different levels of overlap from full overlap (step=1) to minimum overlap (step=3 for $r=4$, that is just one voxel overlap between neighbor windows). In table 2 we can observe that the best results are obtained with full overlap as expected but at the expense of a high processing time. We can also notice that the accuracy differences are really small for the different levels of patch overlap while the processing times are significantly reduced. This can be explained by the fact that the whole group of selected patches is jointly denoised so multiple contributions to every voxel comes from different groups which makes the approach already quite overcomplete. We decided to set the default step value to 3 since it was found to be the most cost-efficient parameter value.

Table 2. PSNR results for different overlapping levels.

Method	Noise level					Average	Time(s)
	1%	3%	5%	7%	9%		
Noisy	39.99	30.46	26.02	23.10	20.91	28.10	
NL-PCA (step=1)	44.85	38.99	36.46	34.77	33.47	37.71	3090
NL-PCA (step=2)	44.83	38.97	36.44	34.76	33.45	37.69	576
NL-PCA (step=3)	44.80	38.93	36.39	34.70	33.39	37.64	169
PRI-NL-PCA (step=1)	45.24	39.44	36.74	34.99	33.65	38.01	3160
PRI-NL-PCA (step=2)	45.23	39.43	36.72	34.98	33.64	38.00	647
PRI-NL-PCA (step=3)	45.20	39.40	36.69	34.94	33.61	37.97	288

3.3. Noise estimation validation

To validate the proposed PCA-based local noise estimation methods a set of experiments were performed. We used the error ratio (ER) and mean error ratio (MER) to measure the different methods noise accuracy for stationary and spatially varying noise respectively.

$$ER = |1 - \hat{\sigma}/\sigma| \quad (13)$$

$$MER = \frac{1}{|\Omega|} \sum_{\forall i \in \Omega} |1 - \hat{\sigma}_i/\sigma_i| \quad (14)$$

where $\hat{\sigma}$ and σ are the estimated and real global noise standard deviation.

3.3.1. Stationary Gaussian noise

In the first experiment, we corrupted the brainweb phantom with different levels of homogenous Gaussian noise. Table 3 shows the noise estimation results when using the compared methods for the 5 different noise levels of Gaussian noise (the image noise level was computed averaging all local estimates). As can be noticed both methods obtained accurate results for medium and high noise levels. The best method over all noise levels was the one based on the trimmed median (eq. 9) as expected due to its ability to estimate the noise level even at low noise conditions.

Table 3. Comparison of the different noise estimation schemes (ER)

Method	Noise level					Average
	1%	3%	5%	7%	9%	
Median (Eq. 8)	0.2100	0.0715	0.0474	0.0395	0.0367	0.0810
Trimmed median (Eq. 9)	0.1141	0.0490	0.0387	0.0356	0.0345	0.0544

3.3.2. Spatially varying Gaussian noise

Although the proposed noise estimation method obtained good results estimating the global noise level of the images, its real potential is its ability to accurately estimate the local noise level present in an image with spatially varying noise patterns. To highlight this point we have compared the proposed method with a related recently proposed local noise estimation method (Maggioni and Foi, 2012). This method, based on the Discrete Cosine Transform (DCT), uses high frequency components of a local set of patches to locally estimate the noise level. This noise estimation method is used internally in an adaptive version of the BM4D denoising method (Maggioni and Foi, 2013). We will refer to this adaptive version as ABM4D to differentiate it from the non-adaptive method BM4D.

During our experiments, stationary and spatially varying conditions were analyzed. In table 4 we can compare the ER results for the proposed method and the ABM4D method for different levels of homogenous Gaussian noise. As can be noticed the proposed method provides more accurate estimates of the noise level for all the considered cases. Most significant differences can be found at low noise levels. This can be understood taking into consideration the fact that the DCT estimations are affected by the overlapping of signal and noise contributions at high frequencies.

Table 4. Comparison of the two different noise estimation schemes (ER)

Method	Noise level					ER
	1%	3%	5%	7%	9%	Average
ABM4D	0.3700	0.1171	0.0729	0.0576	0.0525	0.1340
NL-PCA (Eq. 7)	0.1141	0.0490	0.0387	0.0356	0.0345	0.0544

To evaluate the compared methods over spatially varying noise conditions a new experiment was performed but this time using a spatially varying noise field similar to those that can be found on parallel imaging (see figure 5). To generate the noise field a modulation map with factors 1 to 3 was multiplied with different levels of Rician noise (1% to 9%). In this case the MER measure was used to compare local noise estimations. Table 5 summarizes the results of this experiment. The proposed method obtained the best results for all the noise levels.

Table 5. Comparison of the two different noise estimation schemes for non stationary noise (MER)

Method	Noise level					MER
	1-3%	3-9%	5-15%	7-21%	9-27%	Average
ABM4D	0.2115	0.0715	0.0540	0.0527	0.0549	0.0889
NL-PCA (Eq. 7)	0.0765	0.0409	0.0370	0.0363	0.0365	0.0454

In figure 5 a visual comparison of the results of the compared methods can be performed for both stationary and spatially varying noise cases. The normalized local noise estimation was obtained dividing the estimated noise by the real noise at each point. Perfect match between estimated noise and real noise should produce a normalized value equal to 1, so deviations from this value represents local under and over estimations of the noise level.

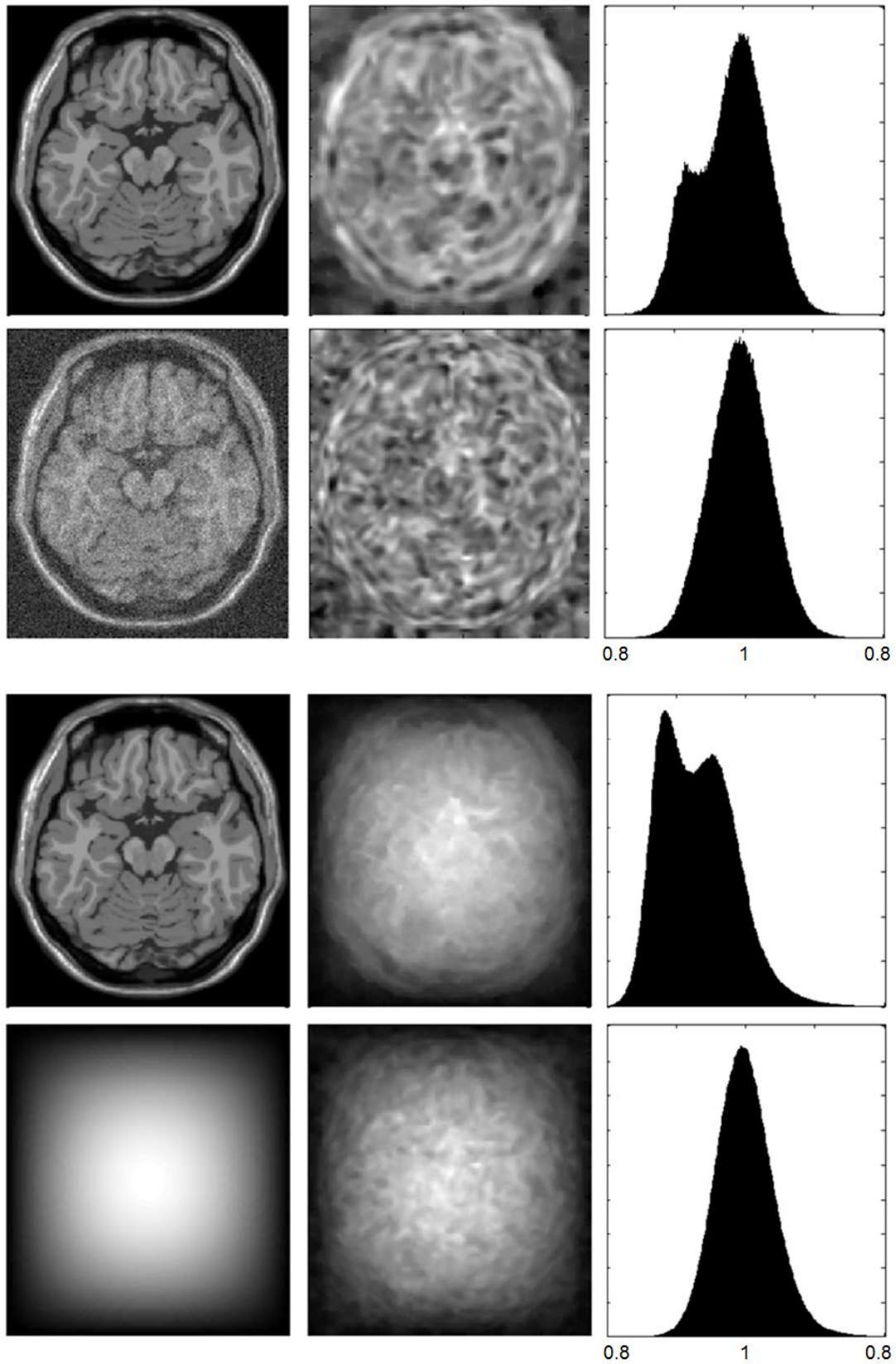


Figure 5. Comparison of ABM4D and NL-PCA noise estimation methods for homogeneous (two first rows) and inhomogeneous (two last rows) Gaussian noise fields. From left to right. First row: Noise free image, ABM4D noise estimation and normalized local noise estimation distribution. Second row: Noisy image, NL-PCA noise estimation and normalized local noise

estimation distribution. Third row: Noise free image, ABM4D noise estimation and normalized local noise estimation distribution. Fourth row: Applied inhomogeneous noise field, NL-PCA noise estimation and normalized local noise estimation distribution.

3.3.3. Stationary Rician noise estimation

Since MR images are typically corrupted with Rician noise, we performed several experiments to evaluate the Rician noise estimation method described in section 2.4. We compared the method based on Koay approach (Koay and Basser, 2006) with our new mapping based approach (eq. 9). We also compared two different options to estimate the original noise field prior the Rician correction, 1) using the NL-PCA noise estimation (eq. 7) and 2) using the local standard deviation of the image residuals (difference between noisy and NL-PCA filtered images). In this later case the local standard deviation was estimated using a local region of 3x3x3 voxels and the resulting noise field was multiplied by a experimentally estimated correction factor (1.05) to compensate the noise underestimation in the residuals to compensate the remaining noise present in the filtered images. The advantage of using the residual image can be explained by the fact that in the filtering process each point is estimated using multiple contributions providing a good approximate of the noise free image which contributes to obtain a more stable and regular noise field estimation. In table 6 the ER results are presented for the different options commented for several levels of homogenous Rician noise (in this case we used a wider noise range to further explore noise underestimation effects at very high noise conditions).

Table 6. Comparison of the different Rician correction methods for homogeneous noise (ER). No correction stands for the NL-PCA noise estimation without any bias correction.

Method	Noise level					Average
	1%	7%	15%	23%	29%	
No correction	0.0468	0.1746	0.2194	0.2548	0.2767	0.1944
Koay	0.0300	0.1131	0.1386	0.1585	0.1725	0.1166
Koay residuals	0.1660	0.1243	0.1225	0.1308	0.1401	0.1367
Mapping (Eq. 11)	0.0518	0.0438	0.0579	0.0688	0.0760	0.0597
Mapping residuals (Eq. 11)	0.1029	0.0432	0.0200	0.0070	0.0005	0.0347

In Figure 6 the estimates of each method for different noise levels are shown. As can be seen, the proposed mapping method based on the image residuals provides acceptable estimates while the other methods tend to underestimate the amount of noise for medium and high noise levels.

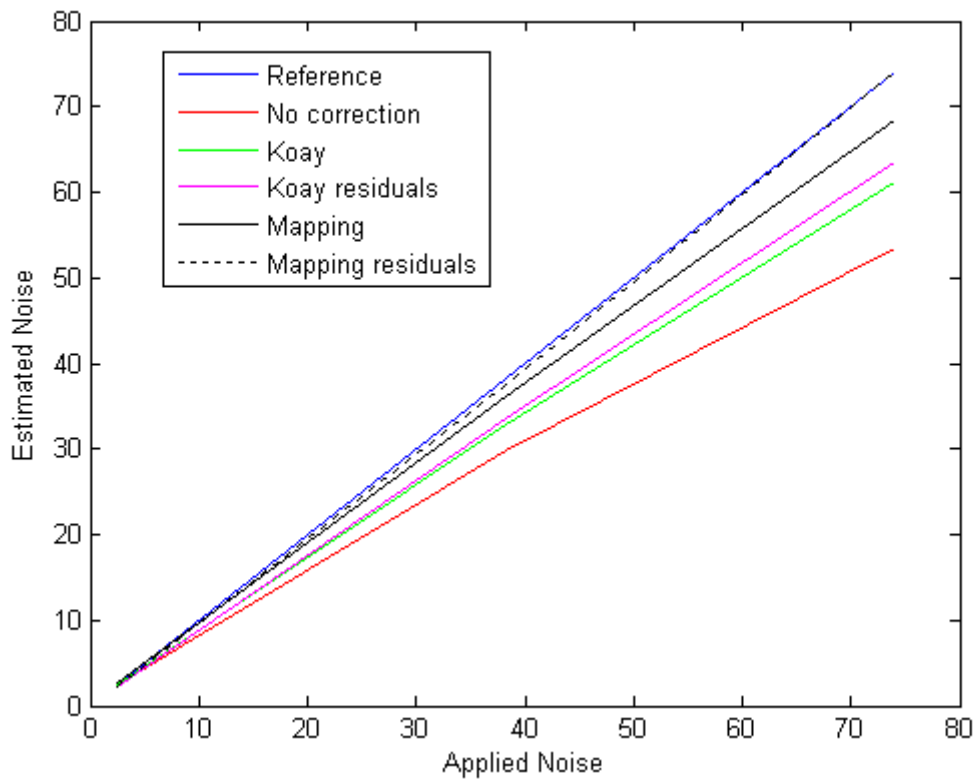


Figure 6. Comparison of different noise estimation methods (Blue line represents the perfect estimation while red line represents the NL-PCA estimation without any underestimation correction). Most of compared methods underestimated the noise variance (especially at low SNR areas) while the proposed mapping technique (using image residuals) provides the most accurate estimation.

The proposed mapping approach provides more accurate noise estimation than Koay approach (applied to both NL-PCA noise estimation and residual based estimation) for all noise levels. The mapping method based on the image residuals gave the lower global error among all compared methods. Therefore, we choose it as our default Rician noise estimation method due its improved overall performance. Figure 7 shows a visual example of output of the different compared methods for stationary Rician noise.

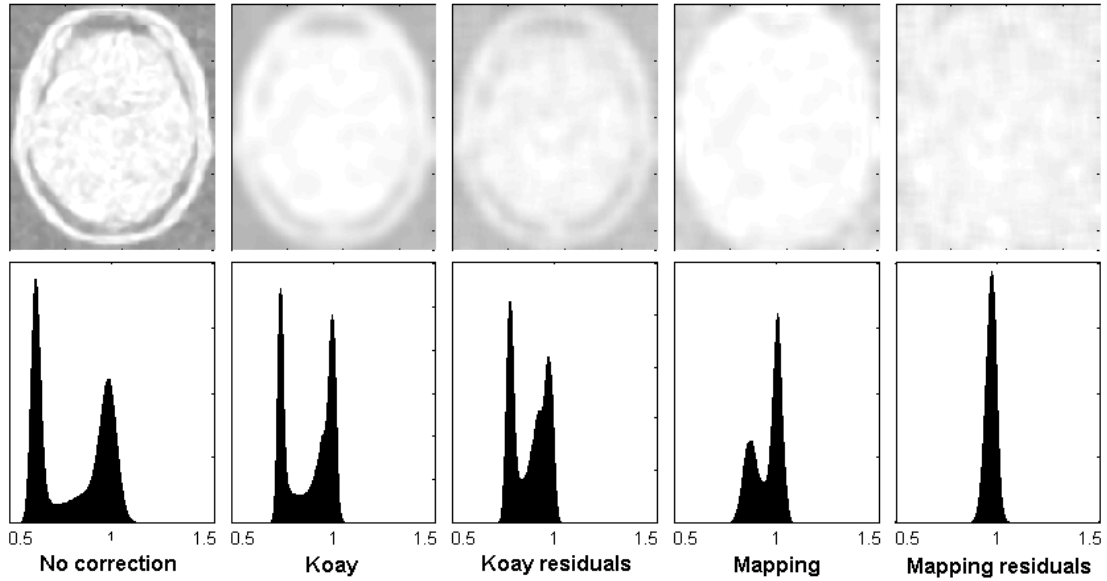


Figure 7. Example of stationary Rician noise estimation results (9%). The noise fields are shown in the $[0,1]$ range after dividing the estimated noise field by the real noise field. From left to right. First column: NL-PCA without Rician correction and corresponding histogram. Second column: NL-PCA output with Koay correction and corresponding histogram. Third column: NL-PCA residual-based noise estimation with Koay correction and corresponding histogram. Fourth column: NL-PCA output, with the proposed mapping correction and corresponding histogram. Fifth column: NL-PCA residual-based noise estimation with the proposed mapping correction and corresponding histogram.

The proposed residual based mapping approach method was compared with the ABM4D method. Table 7 shows the noise estimation results for stationary Rician noise. The proposed method obtained the best results in all the cases.

Table 7. Comparison of the two different noise estimation schemes for different levels of stationary Rician noise (ER).

Method	Noise level					Mean
	1%	3%	5%	7%	9%	
Mapping residuals (Eq. 11)	0.1029	0.0661	0.0514	0.0432	0.0361	0.0599
ABM4D	0.4965	0.1860	0.1388	0.1315	0.1387	0.2183

3.3.4. Spatially varying Rician noise estimation

The proposed residual based mapping approach method was also compared with the ABM4D method for spatially varying noise conditions. In this case, we used also a simulated noise field similar to those that can be found on parallel imaging. To generate the noise field a modulation map with factors 1 to 3 was multiplied with different levels of Rician noise (1% to 9%). Table 8 shows the noise estimation results for the two compared methods. The proposed method obtained the best results in all the considered cases.

Table 8. Comparison of the two different noise estimation schemes for different levels of spatially varying Rician noise (MER).

Method	Noise level					Mean
	1-3%	3-9%	5-15%	7-21%	9-27%	
NL-PCA	0.0850	0.0517	0.0400	0.0356	0.0355	0.0496
ABM4D	0.3524	0.1781	0.1745	0.1868	0.2012	0.2186

3.4 Methods comparison

We compared the proposed methods with *state-of-the-art* methods in MRI denoising. Specifically, for stationary noise, we used the ODCT and PRI-NLM methods (Manjón et al., 2012) and the BM4D (Maggioni et al., 2013a) method. The SANLM filter (Manjón et al., 2010) and the adaptive BM4D (ABM4D) (Maggioni et al., 2013b) were used for the spatially varying noise case.

In the experiments, the exact level of noise added to the images was supplied to the ODCT, PRI-NLM, ONL-PCA, OPRI-NL-PCA and BM4D methods while NL-PCA, PRI-NL-PCA, SANLM and ABM4D methods directly estimated the noise level internally (ONL-PCA and OPRI-NL-PCA are the oracle corresponding versions where the true known noise level was supplied to evaluate the effect of the noise estimation in these methods). PSNR and SSIM measures were obtained only from the foreground areas to avoid background effects.

In table 9 shows the results for stationary Gaussian and Rician noise. As can be noticed the proposed PRI-NL-PCA method obtained the best results in all the cases (note also that the NL-PCA method also improved the BM4D method in all the cases). From table 9, it can be observed that NL-PCA and PRI-NL-PCA results are nearly the same as their Oracle versions highlighting the good behavior of the noise estimation process. A visual example of these results can be observed at figure 8.

Table 9. PSNR and SSIM results of the compared methods for stationary noise (Gaussian and Rician).

Noise	Filter	Noise level					
		1%	3%	5%	7%	9%	Average
Gauss.	Noisy	39.99 0.970	30.46 0.814	26.02 0.656	23.10 0.530	20.91 0.433	28.10 0.681
	ODCT	43.78 0.992	37.53 0.971	34.88 0.951	33.18 0.932	31.91 0.913	36.27 0.952
	PRI-NLM	44.22 0.993	38.34 0.976	35.58 0.959	33.75 0.940	32.37 0.922	36.85 0.958
	ONL-PCA	44.80 0.993	38.93 0.978	36.39 0.964	34.70 0.949	33.39 0.935	37.64 0.964
	NL-PCA	44.80 0.994	38.97 0.979	36.40 0.964	34.67 0.948	33.32 0.931	37.63 0.963
	OPRI-NL-PCA	45.20 0.994	39.40 0.981	36.69 0.968	34.94 0.955	33.61 0.941	37.97 0.968
	PRI-NL-PCA	45.38 0.994	39.33 0.981	36.63 0.968	34.90 0.955	33.58 0.941	37.96 0.968
	BM4D	44.02 0.992	38.35 0.975	35.91 0.960	34.31 0.945	33.10 0.930	37.14 0.960
Rician	Noisy	40.00 0.970	30.49 0.815	26.09 0.656	23.20 0.529	21.04 0.431	28.16 0.680
	ODCT	42.96 0.991	37.38 0.970	34.70 0.949	32.90 0.927	31.53 0.905	35.89 0.948
	PRI-NLM	44.14 0.993	38.28 0.976	35.42 0.957	33.47 0.935	31.98 0.913	36.66 0.955
	ONL-PCA	44.80 0.993	38.89 0.978	36.31 0.963	34.53 0.957	33.11 0.925	37.53 0.962
	NL-PCA	44.79 0.994	38.90 0.978	36.23 0.962	34.37 0.943	32.88 0.923	37.43 0.960
	OPRI-NL-PCA	45.20 0.994	39.35 0.981	36.59 0.967	34.75 0.952	33.28 0.935	37.83 0.966
	PRI-NL-PCA	45.31 0.994	39.34 0.981	36.58 0.967	34.74 0.952	33.28 0.935	37.85 0.966
	BM4D	44.09 0.992	38.35 0.975	35.84 0.959	34.17 0.942	32.88 0.924	36.99 0.958

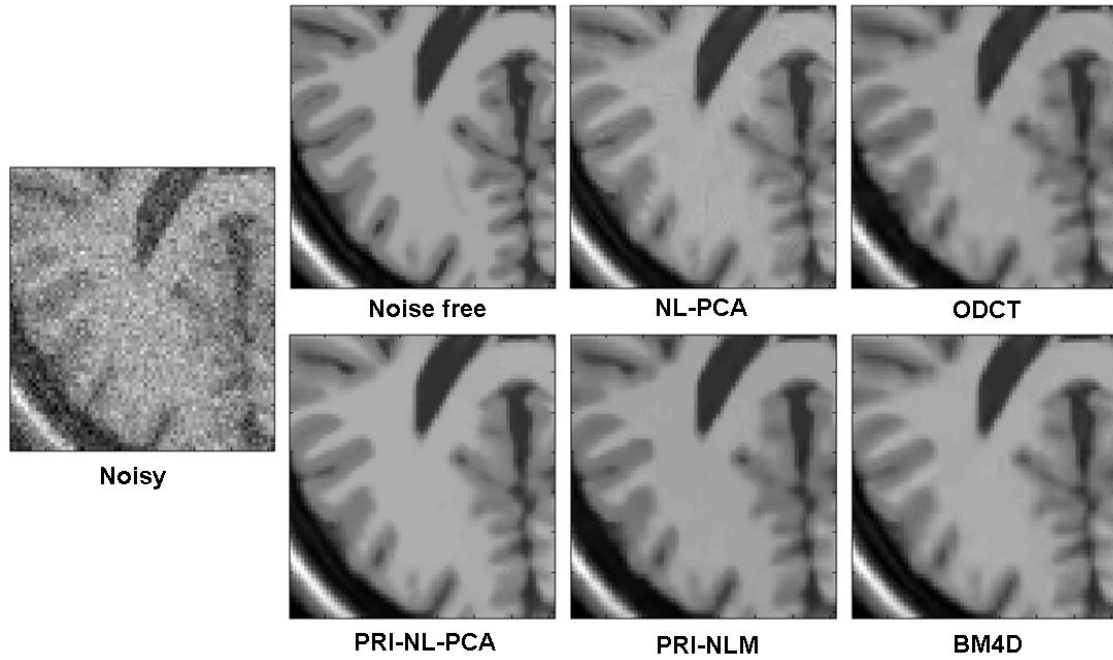


Figure 8. Example results of the compared filters for 9% of Rician noise. A Closed up is shown to better appreciate the differences between compared methods (the method differences can be better appreciated at sulcus areas).

In table 10 the results for spatially varying Gaussian and Rician noise are presented. The proposed PRI-NL-PCA method obtained the best results in almost all the cases. Although ABM4D method showed a good behavior for high levels of Gaussian noise it did not perform as well for Rician noise (probably due to an inaccurate bias correction). A visual example of these results can be observed at figure 9.

Table 10. PSNR and SSIM results of the compared methods for spatially varying noise.

Noise	Filter	Noise Level					
		1-3%	3-9%	5-15%	7-21%	9-27%	Average
Gauss.	Noisy	34.34 0.900	24.80 0.621	20.36 0.442	17.44 0.328	15.26 0.253	22.44 0.508
	ONL-PCA	41.60 0.987	35.94 0.959	33.23 0.928	31.41 0.897	30.07 0.867	34.45 0.928
	NL-PCA	41.66 0.987	35.95 0.958	33.17 0.925	31.31 0.891	29.92 0.857	34.40 0.924
	OPRI-NL-PCA	42.19 0.989	36.33 0.965	33.53 0.939	31.59 0.911	30.10 0.882	34.75 0.937
	PRI-NL-PCA	42.25 0.989	36.30 0.965	33.52 0.939	36.61 0.911	30.16 0.883	34.77 0.937
	ABM4D	40.45 0.980	35.48 0.960	33.10 0.930	31.48 0.900	30.24 0.870	34.15 0.928
	SANLM	40.38 0.980	34.50 0.940	31.57 0.890	29.61 0.830	28.11 0.780	32.83 0.884
Rician	Noisy	34.35 0.900	24.87 0.621	20.50 0.441	17.64 0.325	15.50 0.247	22.57 0.507
	ONL-PCA	41.59 0.987	35.87 0.958	32.99 0.925	30.93 0.890	29.28 0.854	34.13 0.923
	NL-PCA	41.64 0.987	35.77 0.956	32.74 0.917	30.48 0.873	28.42 0.824	33.81 0.911
	OPRI-NL-PCA	42.18 0.989	36.20 0.964	33.16 0.933	30.92 0.897	29.22 0.861	34.34 0.930
	PRI-NL-PCA	42.23 0.989	36.19 0.964	33.15 0.934	30.87 0.897	28.83 0.856	34.25 0.928
	ABM4D	40.43 0.980	34.41 0.940	31.27 0.890	28.80 0.820	26.55 0.740	32.29 0.874
	SANLM	40.28 0.980	34.29 0.940	31.16 0.870	28.73 0.810	26.43 0.740	31.18 0.868

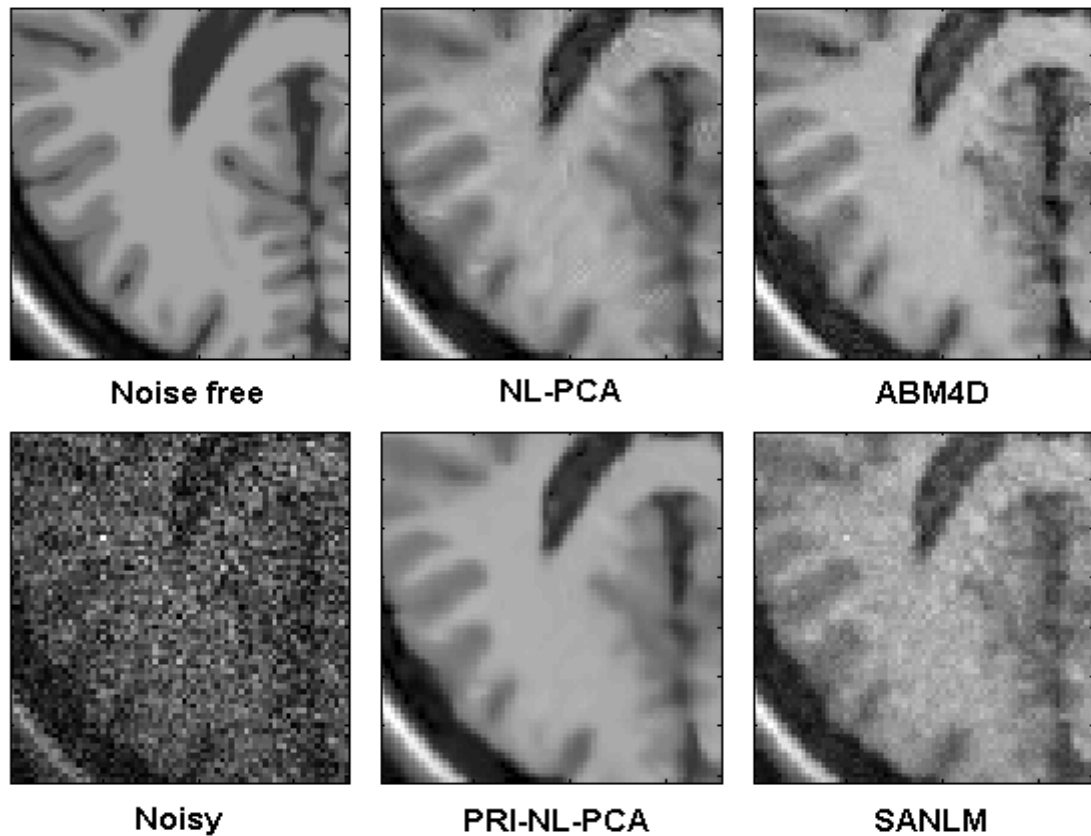


Figure 9. Example results of the compared filters for 9-27% of Rician noise. A Closed up is shown to appreciate the differences between compared methods. Note that NL-PCA method showed some artifacts for very high levels of noise due to non-cancelled components. Note though that the PRI-NL-PCA method does not show any artifact due the different behavior of the averaging process compared to the truncation PCA based process.

Finally, the processing times of the different compared methods were analyzed. The faster method was the ODCCT method with just 5 seconds on average followed by the PRI-NLM with 45 seconds. The SANLM took around 300 seconds. The proposed NL-PCA and PRI-NL-PCA methods took 185 and 320 seconds respectively while the BM4D took 567 seconds when the noise level was externally supplied to the method and 1900 seconds when it was internally estimated from the data (we should note here that the increased processing time of ABM4D may be caused by implementation issues since authors reported that ABM4D has only a slightly higher processing time than BM4D).

Real data comparison

To compare the methods on real clinical data two datasets were used. The first was an MP-RAGE T1w volumetric sequence from OASIS dataset acquired on a Siemens 1.5T Vision scanner (Erlangen, Germany) with TR = 9.7 ms, TE = 4 ms, TI = 20 ms, TD = 200 ms, flip angle = 10° , voxel resolution = $1 \times 1 \times 1.25 \text{ mm}^3$ and 256x256x128 voxels.

We compared visually the proposed PRI-NL-PCA method with the BM4D method since the noise in this volume is expected to be stationary. The stationary noise level in this case (2%) was estimated using the Rician noise estimator proposed by [Coupe et al \(2010\)](#). BM4D method used the estimated noise level provided by the Coupe's method while the PRI-NL-PCA method internally estimated the noise level as previously described. The filtering results for this first dataset are shown in Figure 10. Both methods performed very well on this dataset (the BM4D method seems to slightly over blur sulcal areas). The processing time for this dataset was 240 seconds for PRI-NL-PCA method while the BM4D method took 502 seconds.

The second dataset was obtained with a SENSE T1w volumetric sequence from Quirón Hospital of Valencia (Spain) acquired on Philips Achieva 3 Tesla scanner (Netherlands) with TR=9.5 ms, TE=4.6 ms and flip angle= 8° , 256x256x120 voxels and voxel resolution of $0.96 \times 0.96 \times 1 \text{ mm}^3$.

Figure 11 enables a visual comparison of the results produced using the PRI-NL-PCA and ABM4D methods over this case with spatially varying noise. The PRI-NL-PCA method removed the noise successfully while preserving fine details of the image, whereas the ABM4D method slightly over smoothed some details. The processing time for this dataset was 227 seconds with the PRI-NL-PCA method and 398 seconds with the ABM4D filter. The reduced processing time of ABM4D method compared to the results obtained with the brainweb phantom may be explained by the fact that background of this volume is set to zero by the scanner due to the use of the SENSE sequence and probably the ABM4D method skipped the calculations at this area thus reducing significantly the processing time.

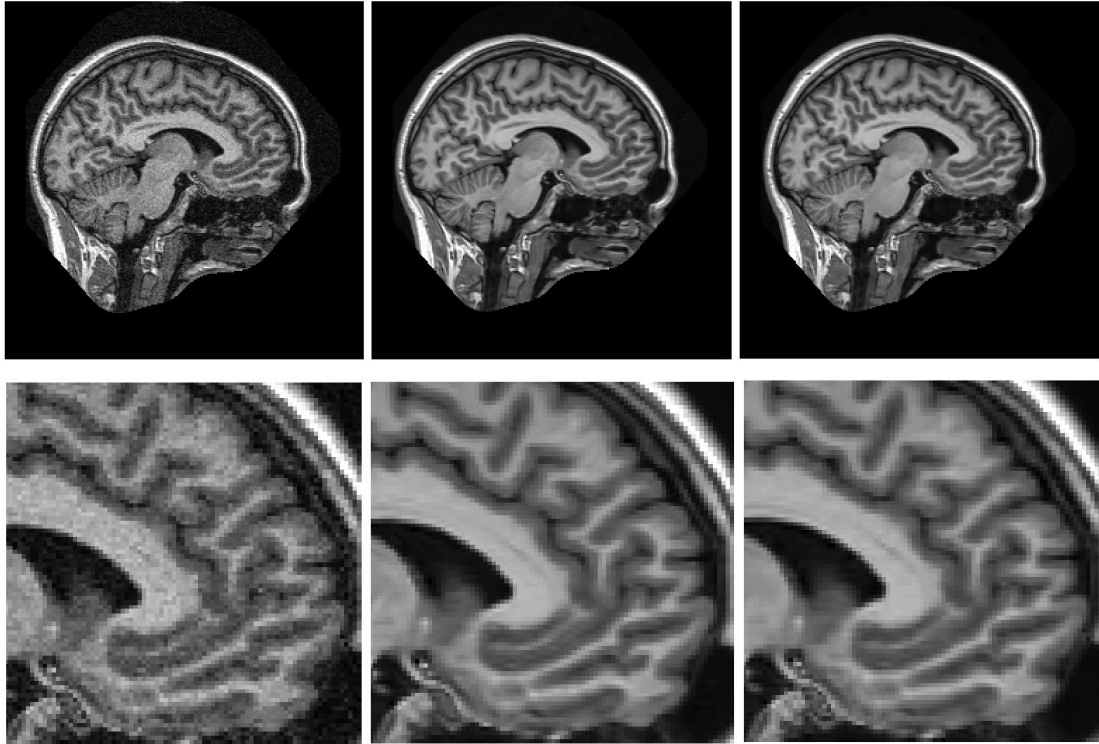


Figure 10. Example of denoising results (stationary noise). From left to right: Original noisy image, PRI-NL-PCA result and BM4D result. Although both methods performed very well the BM4D slightly over blurred the image (this can be noticed in the sulcus areas at the close up).

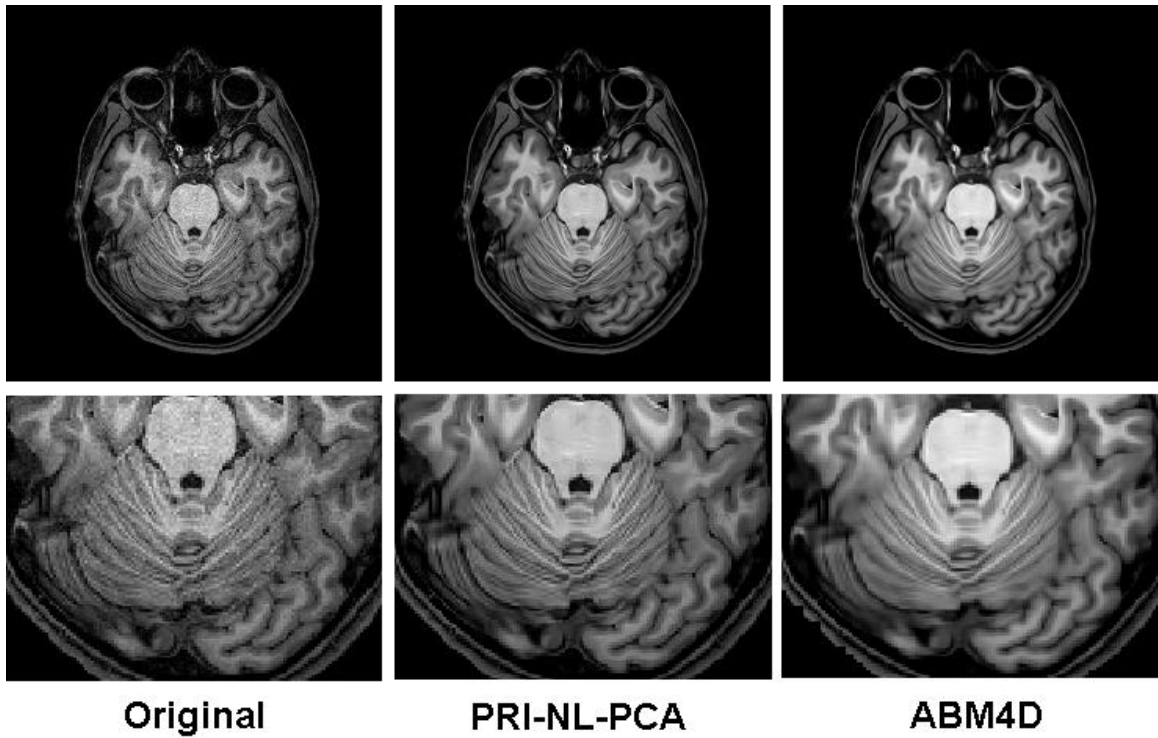


Figure 11. Example of denoising results (spatially varying noise). From left to right: Original noisy image, PRI-NL-PCA result and ABM4D result. Although both methods performed very well, the ABM4D slightly over blurred the image (this can be clearly noticed in the cerebellar area).

4. Discussion

In this paper we have proposed a novel PCA based filter that takes benefit from sparseness properties of groups of similar patches to reduce the noise effectively while minimally affecting the underlying signal. We have also shown that using this filter to create a guide image for the rotationally invariant non-local means filter enables to obtain the best denoising results in the comparison.

The proposed methods have been compared with *state-of-the-art* methods for both stationary and spatially varying noise conditions with Gaussian and Rician noises and obtained the best results. The improved performance of the proposed methods compared to previously proposed methods can be explained by the use of self-similarity and sparseness properties of the images. In fact, grouping similar patches to create a homogenous group allows obtaining a very sparse representation through the use of PCA decomposition. In this sense, our patch selection was improved by performing the patch grouping over a pre-filtered image to make it more robust on very noisy conditions. Besides, differently from other PCA based methods, the use of the pre-filtered guide image obtained with the NL-PCA method enables to accurately estimate the voxel similarities in a rotationally invariant manner that naturally results in a very effective noise reduction within the non-local means strategy.

One of the most significant contributions of this paper is the noise estimation technique within NL-PCA method. Local noise estimation is performed in a local manner from the eigenvalues distribution of the local PCA decomposition with allows to estimate and filter spatially varying noise fields. Furthermore, a novel Rician bias correction technique has been introduced that improves original signal estimation. This technique not only enables the estimation of the local noise level but also enables to automatically estimate the number of significant components to be retained in a fully automatic manner. It's worth noting that this technique can be applied to many other problems where the number of components has to be estimated (for example for dimensionality reduction assuming a random behavior of the non-significant variability sources). We have also presented a novel method for correcting the Rician noise underestimation. Despite the simplicity of this method it has been experimentally demonstrated its ability to obtain very fast and accurate local noise estimations improving a previous existing method.

From an efficacy point of view, the proposed PRI-NL-PCA method has been shown to be almost two times faster than BM4D method and six times faster than the ABM4D method. The proposed PRI-NL-PCA method obtained an average improvement of almost 1 dB compared to the state-of-the-art BM4D method for stationary Rician noise. From a practical point of view, the proposed method can be applied to both stationary of spatially varying noise cases in a fully automatic manner that makes it ideal for a use within a preprocessing pipeline for automated MRI analysis tasks.

It should be noted though that the proposed methods in this paper assume the presence of white noise in the images. This condition may not be satisfied when using acceleration techniques such as partial Fourier or compressed sensing. In these cases, the methods proposed in this paper cannot be directly applied due to the correlated nature of the noise. This situation will be studied in future works.

Acknowledgments

We are grateful to Dr. Matteo Mangioni and Dr. Alessandro Foi for their help on running their BM4D method in our comparisons. We want also to thank Dr. Luis Martí-Bonmatí and Dr. Angel Alberic from Quirón Hospital of Valencia for providing the real clinical data used in this paper. This study has been carried out with financial support from the French State, managed by the French National Research Agency (ANR) in the frame of the Investments for the future Programme IdEx Bordeaux (ANR-10-IDEX-03-02), Cluster of excellence CPU and TRAIL (HR-DTI ANR-10-LABX-57).

References

Aharon M, Elad M, Bruckstein A M. 2006. K-SVD: an algorithm for designing over complete dictionaries for sparse representation. *IEEE Trans. Signal Process.*, 54:4311–4322.

Aja-Fernandez, S., Tristan, A., Alberola-Lopez, C., 2009. Noise estimation in single and multiple coil magnetic resonance data based on statistical models. *Magn Reson Imaging* 27, 1397-1409.

Bao L, Liu W, Zhu Y, Pu Z, Magnin I. 2008. Sparse Representation Based MRI Denoising with Total Variation. *ICSP2008 Proceedings*

Bao L, Robini M, Liu W, Zhu Y. 2013. Structure-adaptive sparse denoising for diffusion-tensor MRI. *Medical Image Analysis*, 17(4), 442–457.

Bydder M, Du J (2003) Noise reduction in multiple-echo data sets using singular value decomposition. *Magn Reson Imaging* 24(7): 849–856.

Buades A, Coll B and Morel J.M. 2005. A non-local algorithm for image denoising. *IEEE Int. Conf. on Computer Vision and Pattern Recognition (CPVR)* 2, 60–65.

Collins D.L., Zijdenbos A.P., Kollokian V., Sled J.G., Kabani N.J., Holmes C.J. and Evans A.C. 1998. *Design and construction of a realistic digital brain phantom. IEEE Trans. Med. Imaging*, 17, 463–468.

Coupé P., Yger P., Prima S., Hellier P., Kervrann C. and Barillot C. 2008. An optimized blockwise nonlocal means denoising filter for 3-D magnetic resonance images. *IEEE Trans. Med. Imaging*, 27, 425–441.

Coupé P., Manjón J.V., Gedamu E., Arnold D., Robles M. and Collins D.L. 2010. Robust Rician noise estimation for MR images. *Med. Image Anal*, 14, 483–493.

Coupé P, Munz M, Manjón J. V., Ruthazer E., Collins D. L. 2012. A CANDLE for a deeper in vivo insight. *Medical Image Analysis*, 16 (4):849-864.

Deledalle C, Salmon J, Dalalyan A. 2011. Image denoising with patch based PCA: local versus global. *BMVC* 2011

Elad M and Aharon M. 2006. Image Denoising Via Sparse and Redundant representations over Learned Dictionaries, the IEEE Trans. on Image Processing, 15(12), pp. 3736-3745.

Fan Lam S, Babacan D, Haldar JP, Weiner MW, Schuff N, et al. 2013. Denoising diffusion-weighted magnitude MR images using rank and edge constraints. *Magnetic Resonance in Medicine*, 69(6): 1–13.

Guleryuz, O.G., 2003. Weighted overcomplete denoising. In: Proceedings of the Asilomar Conference on Signals and Systems.

He, L., Greenshields, I.R., 2009. A nonlocal maximum likelihood estimation method for Rician noise reduction in MR images. *IEEE Trans Med Imaging* 28, 165-172.

Katkovnik V, Foi A, Egiazarian K, and Astola J. 2010. From local kernel to nonlocal multiple-model image denoising. *Int. J. Computer Vision*, 86(1): 1-32

Kim DW, Kim C, Kim DH, Lim, DH. 2011. Rician nonlocal means denoising for MR images using nonparametric principal component analysis. *EURASIP Journal on Image and video Processing*, 2011:15.

Koay CG and Basser PJ. 2006. Analytically exact correction scheme for signal extraction from noisy magnitude MR signals. *Journal of Magnetic Resonance*; 179: 477-482.

Kwan R.K.-S., Evans A.C. and Pike G.B. 1999. MRI simulation-based evaluation of image-processing and classification methods. *IEEE Trans. Med. Imaging*, 18, 1085–1097.

Mairal J, Elad M, Sapiro G. 2008. Sparse learned representations for image restoration. IASC2008:, Yokohama, Japan

Maggioni M., Katkovnik V., Egiazarian K, Foi A. 2013. A Nonlocal Transform-Domain Filter for Volumetric Data Denoising and Reconstruction., *IEEE Trans. Image Process.*, 22(1),pp. 119-133.

Maggioni M, Foi A. 2012. Nonlocal Transform-Domain Denoising of Volumetric Data With Groupwise Adaptive Variance Estimation. *Proc. SPIE Electronic Imaging (EI)*, 2012, San Francisco, CA, USA.

Manjón J.V., Carbonell-Caballero J., Lull J.J., Garcia-Martí G., Martí-Bonmatí L. and Robles M. 2008. MRI denoising using non-local means. *Med. Image Anal*, 4 , 514–523.

Manjón J.V., Thacker N.A., Lull J.J., Garcia-Martí G., Martí-Bonmatí L., Robles M. 2009. Multicomponent MR Image Denoising. *International Journal of Biomedical imaging*. Article ID 756897.

Manjón J.V., Coupé P., Martí-Bonmatí L., Robles M. and Collins D.L. 2010. Adaptive non-local means denoising of MR images with spatially varying noise levels. *J. Magn. Reson. Imaging*, 31, 192–203.

Manjón J. V., Coupé P., Buades A., Collins D. L., Robles M. 2012. New Methods for MRI Denoising based on Sparseness and Self-Similarity. *Medical Image Analysis*, 16(1): 18-27.

Manjón J.V., Coupé P., Concha L., Buades A., Collins D.L., Robles M. 2013. Diffusion Weighted Image Denoising using overcomplete Local PCA. *PLoS ONE* 8(9): e73021. doi:10.1371/journal.pone.0073021.

Mohan J, Krishnaveni V, Guo Y. 2014. A survey on the magnetic resonance image denoising methods. *Biomedical Signal Processing and Control*, 9, 56–69

Muresan D.D. and Parks T.W. 2003. Adaptive principal components and image denoising. *IEEE Int. Conf. Image Process.*, 1, 101–104.

Nowak R. 1999. Wavelet-based Rician noise removal for magnetic resonance imaging. *IEEE Trans. Image Process*, 8, 1408–1419.

Pan X, Zhang X and Lyu S. 2012. Blind Local Noise Estimation for Medical Images Reconstructed from Rapid Acquisition, *SPIE 2012*. San Diego, CA.

Protter M. and Elad M. 2009. Image Sequence Denoising Via Sparse and Redundant Representations. *IEEE Trans. on Image Processing*, Vol. 18(1), Pages 27-36.

Pyatykh S., Hesser J, and Zheng L. 2013. Image Noise Level Estimation by Principal Component Analysis, *IEEE TIP*, 22, 687-699.

Rajan J, Veraart J, Audekerke J, Verhoye M, Sijbers J. 2012. "Nonlocal maximum likelihood estimation method for denoising multiple-coil magnetic resonance images", *Magn Reson Imaging*, 30,1512-1518.

Rajan J, Den Dekker A, Sijbers J. 2014. A new non local maximum likelihood estimation method for Rician noise reduction in Magnetic Resonance images using the Kolmogorov-Smirnov test. *Signal Processing*, 103,16-23.

Salmon J, Willett R, Arias-Castro E. 2012. A two-stage denoising filter: the preprocessed Yaroslavsky filter. *Statistical Signal Processing Workshop (SSP), 2012 IEEE*, 464-467.

Sijbers J., Poot D. H. J., den Dekker A. J., and Pintjens W. 2007. Automatic estimation of the noise variance from the histogram of a magnetic resonance image. *Physics in Medicine and Biology*, vol. 52(5), pp. 1335-1348.

Tristán-Vega A, García-Pérez V, Aja-Fernández S. 2012. Efficient and Robust Nonlocal Means Denoising of MR Data Based on Salient Features Matching, *Computer Methods and Programs in Biomedicine*. 105(2):131–144.

Van De Ville D. and Kocher M. 2010. Non-Local Means with Dimensionality Reduction and SURE-Based Parameter Selection, *IEEE TIP*, 20(9), 2683-2690.

Vishal Patel, Yonggang Shi, Paul M. Thompson, Arthur W. Toga. 2011. K-SVD FOR HARDI DENOISING. *IEEE International Symposium on Biomedical Imaging: From Nano to Macro*.

Wang Z., Bovik A.C., Sheikh H.R. and Simoncelli E.P. 2004. Image quality assessment: from error visibility to structural similarity. *IEEE Trans. Image Process.*, 13, 600–612.

Wiest-Daesslé N., Prima S., Coupé P., Morrissey S.P. and Barillot C. 2008. Rician noise removal by non-local means filtering for low signal-to-noise ratio MRI: applications to DR-MRI. *MICCAI*, 11, 171–179.

Yaroslavsky, L.P., Egiazarian, K., Astola, J., 2000. Transform domain image restoration methods: review, comparison and interpretation. *TICSP Series #9, TUT*, ISBN 952-15-0471-4.

Zhang L, Dong W, Zhanga D, Shib G. 2010. Two-stage image denoising by principal component analysis with local pixel grouping. *Pattern Recognition*, 43(4),1531-1549.

Zhang, YQ ; Ding, Y ; Liu, JY ; Guo, ZM. 2013. Guided image filtering using signal subspace projection. *IET Image Processing*, 7(3), 270-279.

Zhang, YQ ; Liu, JY ; Li, MD ; Guo, ZM. 2014. Joint image denoising using adaptive principal component analysis and self-similarity, Information Sciences, 259,128-141.